ELSEVIER

Fluid Phase Equilibria 121 (1996) 111–123

FLUID PHASE EQUILIBRIA

Improved modelling of vapour–liquid equilibria up to the critical region. Application to the CO_2–CH_4–N_2 system

R. Thiéry *, J. Dubessy

CREGU, Centre de Recherche sur la Géologie des Matières Minérales et Energétiques, BP 23, 54501-Vandoeuvre-les-Nancy Cedex, France

Received 30 June 1995; accepted 30 January 1996

Abstract

A new procedure for extending the applicability of cubic EOS to critical conditions is described. This method requires to determine two sets of optimum binary interaction parameters for the non-critical and critical parts of *PTx* experimental data of binary systems. The effective binary interaction parameters are calculated by interpolation between these two sets of binary interaction parameters. The interpolation factor is a function of a distance from critical conditions, which is evaluated from an *a priori* calculation of the molar volumes of coexistent liquid and vapour. The algorithm is shown to improve the prediction of the Soave–Redlich–Kwong equation of state in the ternary CO_2–CH_4–N_2 system. Application conditions of this approach to other systems are discussed.

Keywords: Theory; Equation of state; Cubic; Critical; CO_2–CH_4–N_2 mixtures

1. Introduction

Cubic equations of state (EOS) are successful for predicting fluid phase equilibria of nonpolar mixtures with a few number of parameters. However, they cannot be used for critical conditions, as they overestimate the extent of the liquid–vapour immiscibility. Any calculated liquid–gas isotherm of a binary system deviates largely from the experimental data in the critical region on a *Px* diagram. This is a serious problem when an accurate modelling of phase equilibria is required, e.g. for fluid inclusion studies in the CO_2–CH_4–N_2 system [1,2]. Several attempts have been proposed for improving the predictions for the CO_2–CH_4–N_2 system. A first solution is to use other mixing and combining rules [3], or to incorporate more parameters to the equation [3,4]. These methods generally improve the predictions of volumetric properties of fluids, but significant deviations are still observed

* Corresponding author.

0378-3812/96/$15.00 © 1996 Elsevier Science B.V. All rights reserved
PII S0378-3812(96)03029-4

for the critical conditions. Kreglewski and Hall [5] proposed a non-cubic EOS for the binary CO_2–CH_4 and CO_2–N_2 system, and they applied a semi-empirical correction in the critical regions. However, as it can be seen on their published figures (Figs. 1 and 5, their article), their model introduces unrealistic discontinuity and dissymmetry in the critical part of isothermal Px curves.

It is well known that the theoretical basis of a cubic EOS is not adequate for predicting the properties of a system near its critical state. Indeed, cubic EOS are based on the assumption of the "mean molecular field", which assumes that the potential energy field exerted around a molecule is practically the same for each molecule of a phase. This simplification is clearly not valid for critical conditions, which are characterized by large density fluctuations at the molecular scale. Surprisingly, it remains possible to correlate experimental critical points of a binary system with a simple cubic EOS [6,7]. However, this requires the use of binary interaction parameters (BIP), whose values are largely different from those used for liquid–vapour equilibria, and therefore, are not suitable outside the critical region. The aim of this paper is to show that cubic EOS are capable of representing vapour–liquid equilibria, both for critical and non-critical conditions, by building a model whose BIP are allowed to vary as a function of the distance from critical conditions [8–10]. An interpolation parameter is used in order to join the two areas of applicability of cubic EOS without discontinuity. First, the definition of the interpolation factor is given. Two sets of optimum BIP are determined from experimental data. Then, the improvements on the prediction of phase equilibria are reported.

2. The algorithm

The Soave–Redlich–Kwong (SRK) EOS [11] has been chosen as a basis for modelling liquid–gas equilibria of the CO_2–CH_4–N_2 system. The usual quadratic and combining rules are used for both a and b parameters of the SRK EOS [12]:

$$a = \sum_i \sum_j x_i x_j a_{ij} (1 - k_{a,ij}) \tag{1}$$

$$b = \sum_i \sum_j x_i x_j b_{ij} (1 - k_{b,ij}) \tag{2}$$

$$a_{ij} = \sqrt{a_i a_j} \tag{3}$$

$$b_{ij} = (b_i + b_j)/2 \tag{4}$$

where $k_{a,ij}$ and $k_{b,ij}$ are the binary interaction parameters (BIP) respectively on the a and b parameters, which are specific to the interactions between species i and j.

The SRK EOS has been successfully applied to the CO_2–CH_4–N_2 system with only one BIP on the a parameter [1,2], except in the critical and retrograde condensation regions. The pressure is strongly overestimated in the critical region. Pressure discrepancies may be as large as 25 bar for the CO_2–N_2 system at -30°C (Fig. 1) and the CO_2 content of the critical point is always underestimated (up to 10%) for the CO_2–N_2 and the CO_2–CH_4 system (Fig. 1(A) and 1(B)). Therefore, an improvement of the EOS is necessary for quantitative use. However, the CH_4–N_2 system is well predicted by the SRK EOS [1]. Discrepancies near critical points are not important enough and do not justify a modification of the model for the CH_4–N_2 system.

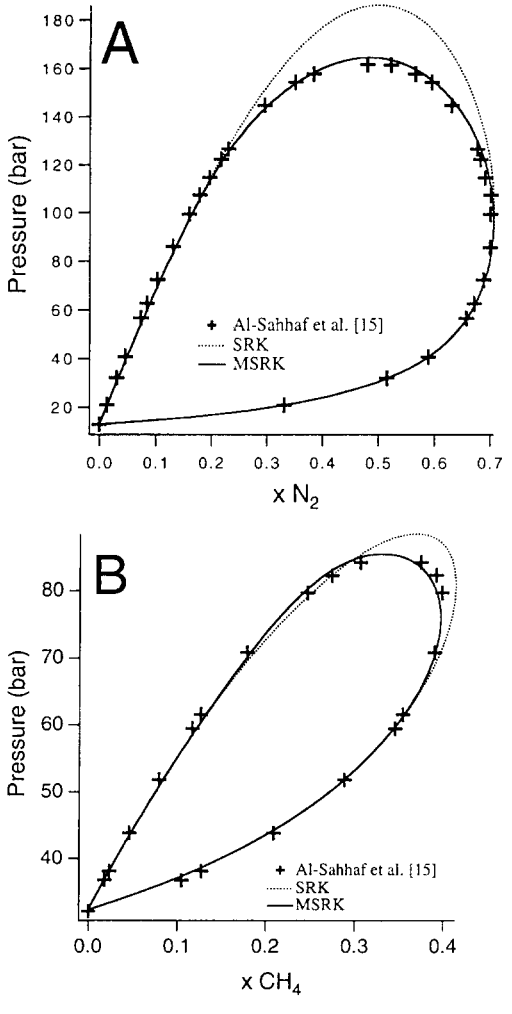

Fig. 1. Isothermal P_x projections of the liquid-vapour immiscibility region. A, at -33.15°C for the CO_2–N_2 system; B, at -3.15°C for the CO_2–CH_4 system. The experimental data are those of Al-Sahhaf et al. [15]. The dotted curve is for the SRK EOS, whereas the solid curve is for the MSRK EOS, with variable BIP.

As stated above, a new interpolation parameter, denoted as ξ, is introduced for calculating effective BIP, as follows

$$k_{a,ij} = \xi k^{c}_{a,ij} + (1-\xi)k^{nc}_{a,ij} \tag{5a}$$

$$k_{b,ij} = \xi k^{c}_{b,ij} + (1-\xi)k^{nc}_{b,ij} \tag{5b}$$

where superscripts *nc* and *c* denote non-critical and critical conditions respectively. ξ takes values ranging between 0 (non-critical state) and 1 (critical state); $k^{nc}_{a,ij}$, $k^{nc}_{b,ij}$, $k^{c}_{a,ij}$, and $k^{c}_{b,ij}$ are BIP, determined independently by fitting the EOS with experimental data. ξ should represent a function of the distance of the state of the fluid with respect to critical conditions. We can make use of the fact that molar volumes of the gas and liquid phases become almost equal for near-critical conditions.

Accordingly, ξ is expressed as a function of v_r, the ratio of the molar volume of the gas (v_G) to the molar volume of the coexistent liquid (v_L):

$$v_r = \frac{v_G}{v_L} \tag{6}$$

where v_G and v_L are calculated with the classical SRK EOS ($\xi = 0$).The following threshold function is used to describe the dependence of the ξ parameter to v_r:

$$\xi = \exp\left(-A(s - v_r)^2\right) \; for \; v_r > s \tag{7a}$$

$$\xi = 1.0 \; for \; v_r < s \tag{7b}$$

As required, this function is equal to 1 for critical states and to 0 for non-critical conditions. A function, that mimics a half gaussian bell curve, has been used for the transition region between the critical and non-critical fields. This function has been found to give the best results, whereas other tested functions, such a linear or a parabolic ramp, fail to reproduce adequately the shape of the isothermal *Px* isotherms. Two parameters are involved for the gaussian transition (Eq. (7)). The first parameter, denoted as s, influences the position of the ramp with respect to v_r values of reduced molar volumes (Eq. (6)). The second parameter, denoted as A, has an influence on the slope of the ramp between critical and non-critical conditions. Values of A and s parameters have been estimated crudely for the CO_2–CH_4–N_2 system from experimental data of the binary subsystems ($A = 0.5$ and $s = 1.05$).

In short, two steps are required for calculating a liquid–vapour equilibrium point. The first one is the calculation of a point with the usual BIP that are suitable in the non-critical part.

$$k_{a,ij} = k^{nc}_{a,ij} \tag{8a}$$

$$k_{b,ij} = k^{nc}_{b,ij} \tag{8b}$$

The molar volumes of the coexistent liquid (v_L) and vapour (v_L) phases are calculated. The interpolation factor ξ is estimated from Eqs. (7a) and (7b). Then, new BIP are calculated from Eqs. (5a) and (5b). These effective BIP are used for calculating the correct liquid–vapour equilibria point. This algorithm has been implemented with thermodynamic calculations packages for calculating *Px* isotherms, *PT* isopleths and other projections of the liquid–vapour immiscibility regions [13,14]. Contrary to the empirical correction proposed by Kreglewski and Hall [5] in the critical region, it is not necessary here to iterate until consistent values of the ξ interpolation factor and the v_r ratio of

Table 1
Binary interaction parameters

Systems	Non-critical part		Critical part	
	k^{nc}_a	k^{nc}_b	k^{c}_a	k^{c}_b
CO_2–N_2	−0.035	0.0	−0.116	−0.071
CO_2–CH_4	0.1	0.0	0.074	−0.051
CH_4–N_2	0.03	0.0	0.03	0.0

molar volumes are obtained. Such iterations would increase a lot the complexity of calculations, and the accuracy of results could not be improved significantly.

3. The fitting of binary interaction parameters in the CO_2–CH_4–N_2 system

Best-fitting k_{ij}^{nc} BIP have been determined in a previous study in the non-critical region [1] from experimental data of the binary systems CH_4–N_2, CO_2–N_2 and CO_2–CH_4 [15–36]. The $k_{b,ij}^{nc}$ values have been set to zero, and the $k_{a,ij}^{nc}$ values are temperature independent (Table 1).

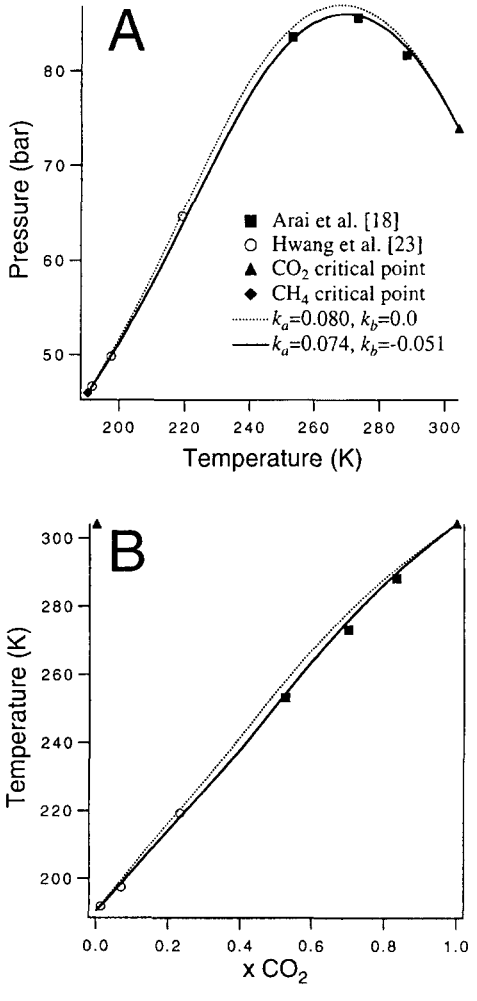

Fig. 2. The critical curve of the CO_2–CH_4 system. A, *PT* projection. B, *Tx* CO_2 projection. Experimental data are those of Arai et al. [18] and Hwang et al. [23]. The dotted curve is the critical line calculated by the SRK EOS with one BIP on the *a* parameter ($k_a^c = 0.08$). A more satisfactory agreement with experimental data is obtained by considering two BIP on the *a* and *b* parameters (solid curve, $k_a^c = 0.074$, $k_b^c = -0.051$).

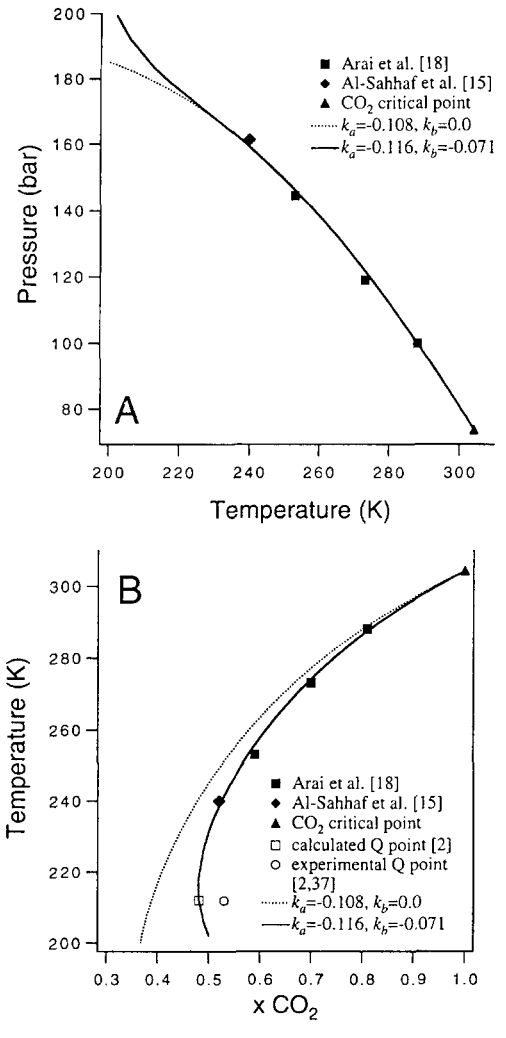

Fig. 3. The critical curve of the CO_2–N_2 system. A, *PT* projection, B, *Tx* projection. Experimental data used for fitting BIP are those of Arai et al. [18] and Al-Sahhaf et al. [15]. The dotted curve is calculated by the SRK EOS by using only one BIP on the *a* parameter ($k_a^c = -0.108$). Closer agreement with experimental data is obtained with two BIP on the *a* and *b* parameters (solid curve, $k_a^c = -0.116$, $k_b^c = -0.071$). The intersection of the CO_2–N_2 critical curve with the CO_2 solid-liquid-gas curve has been calculated with the MSRK EOS at $T = -61.1$°C and $x\ N_2 = 0.53$ (empty square, [2]). This calculated Q point is in fair agreement with the estimation of Kerkhof [37], using synthetic fluid inclusions ($T = -61.2$°C and $x\ N_2 = 0.47$).

Optimum k_{ij}^c BIP have been determined along the critical locus curve for the CO_2–N_2 and the CO_2–CH_4 systems from available experimental data [15,18,23] (see Fig. 2). For this purpose, the minimum of an objective *S* function has been searched by using a minimization routine.

$$S = \sum_{i=1}^{N} \left[\left(\frac{P_i^{\exp} - P_i^{calc}}{P_i^{\exp}} \right)^2 + \left(y_i^{\exp} - y_i^{calc} \right)^2 \right] \tag{9}$$

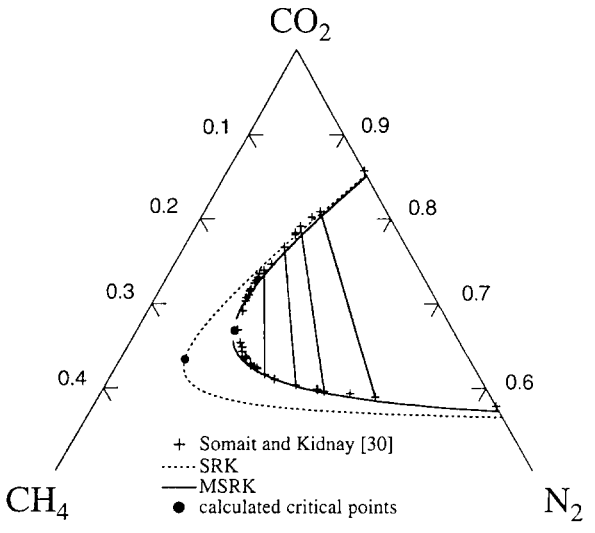

Fig. 4. Isothermal and isobaric liquid-vapour immiscibility region on a ternary CO_2–CH_4–N_2 diagram. The experimental data are those of Somait and Kidnay [30] at −3.15°C and 96.3 bar. The dotted curve is for the SRK EOS, whereas the solid curve is for the MSRK EOS with variable BIP. Calculated critical points and some experimental tie-lines are drawn too.

where y_i^{exp} and y_i^{calc} are the experimental and calculated mole fraction of CO_2 respectively, and P_i^{exp} and P_i^{calc} are the respective experimental and calculated pressures for each experiment i. A first attempt, where only the $k^c_{a,ij}$ BIP was fitted, did not result to a sufficient agreement with experimental data, as it can be seen on PT and Tx projections of the critical curve (dotted curve on Figs. 3 and 4). For our purposes, a close agreement between the model and experimental data is important. Otherwise, unrealistic variations of the isothermal Px immiscibility loops may be produced (as in the work of Kreglewski and Hall [5]). Incorporation of the BIP on the b parameter (Eq. (4)) into the model results in a better agreement (Figs. 3 and 4).

4. Results

Improvements of the prediction of the model on the binary CO_2–CH_4 and CO_2–N_2 systems are shown in Fig. 1(A) and 1(B). As expected, the critical and the retrograde condensation regions are reproduced better. For example, in Fig. 1(A), the critical pressure is overpredicted by more than 25 bar with the SRK EOS, whereas the pressure deviation ($\Delta P = P_{calc} - P_{exp}$) is below 3 bar with our modified Soave–Redlich–Kwong (MSRK) EOS. Comparisons between the SRK and our MSRK EOS are reported in Table 2 for the CO_2–N_2 system and in Table 3 for the CO_2–CH_4 system. Liquid–vapour phase equilibria have been calculated for all available experimental data. For a given temperature and liquid composition, the pressure and the vapour composition were calculated. Results in Tables 2 and 3 have been reported only for the retrograde condensation region and the critical region, i.e. in the fields where the MSRK EOS produces strongly different values from the SRK EOS. The use of our improved model allows the reproduction of experimental data with a better accuracy. Pressure and vapour composition are reproduced with a relative error around the percent for the binary CO_2–CH_4 and CO_2–N_2 systems in the critical region. The method has been tested also for the

Table 2
Accuracies of bubble pressure calculations for the CO_2–N_2 system

References	Temperature	Number of points	AADP [a]		AADy [b]	
	(K)	N	SRK	MSRK	SRK	MSRK
[15]	240.00	4	5.58	0.63	3.02	0.96
[30]	270.00	6	1.88	1.08	2.63	1.06
[32]	273.15	3	4.88	1.29	2.78	0.54
[33]	273.15	3	1.65	1.27	1.10	0.54
[33]	232.85	3	2.44	1.39	1.59	1.65
[17]	223.15	3	3.31	1.95	0.70	0.30
[17]	273.15	2	1.80	1.04	1.14	0.68
All data		24	3.08	1.20	2.03	0.86

[a] $\mathrm{AAD}P = \left[\frac{1}{N}\sum_{i=1}^{N}|P_i^{\exp} - P_i^{cal}|/P_i^{\exp}\right]\times 100$; [b] $\mathrm{AAD}y = \left[\frac{1}{N}\sum_{i=1}^{N}|y_i^{\exp} - y_i^{cal}|\right]\times 100$.

CO_2–CH_4–N_2 ternary system. An isothermal and isobaric projection of the liquid–gas immiscibility is given in Fig. 4. Whereas the CH_4 mole fraction of the critical point is predicted with a deviation of 0.07 by the SRK EOS, the deviation is below 0.01 with the MSRK EOS. Numerical comparisons between the SRK and the MSRK EOS are reported in Table 4 for the ternary system in the critical region. Relative errors on the pressure and vapour composition are below 1.5%. Thus, our model improves significantly too the predictions in the ternary system and no ternary interaction parameters are required.

5. Application to other systems

This method improves the prediction of liquid–vapour equilibria of the CO_2–CH_4–N_2 system with a cubic EOS up to the critical conditions. Such a method could be used for other systems and with other EOS. However, it is important to point out the potential problems and to show how to solve them.

Table 3
Accuracies of bubble pressure calculations for the CO_2–CH_4 system

References	Temperature	Number of points	AADP [a]		AADy [b]	
	(K)	N	SRK	MSRK	SRK	MSRK
[22]	271.48	3	4.35	3.42	0.96	1.16
[24]	253.15	2	1.10	0.26	1.54	0.53
[15]	240.00	7	1.95	1.42	1.0	1.23
[21]	230.00	5	0.91	0.75	0.80	0.85
[21]	250.00	3	1.75	0.70	1.99	1.98
All data		20	1.93	1.33	1.15	1.17

[a] $\mathrm{AAD}P = \left[\frac{1}{N}\sum_{i=1}^{N}|P_i^{\exp} - P_i^{cal}|/P_i^{\exp}\right]\times 100$; [b] $\mathrm{AAD}y = \left[\frac{1}{N}\sum_{i=1}^{N}|y_i^{\exp} - y_i^{cal}|\right]\times 100$

Table 4
Accuracies of bubble pressure calculations for the CO_2–CH_4–N_2 system

References	Temperature (K)	Pressure (bar)	Number of points N	AADP [a]		AADy [b] (N_2)		AADy [b] (CH_4)	
				SRK	MSRK	SRK	MSRK	SRK	MSRK
[15]	220.00	91.19	2	5.01	3.94	0.97	1.03	0.83	0.85
[15]	220.00	121.59	5	3.91	2.86	0.96	0.92	0.73	0.73
[15]	233.15	81.06	3	2.27	1.96	0.12	0.15	0.72	0.77
[15]	240.00	91.19	6	2.30	0.97	0.32	0.33	1.00	0.77
[15]	240.00	121.59	7	2.62	0.45	1.49	0.92	0.55	0.34
[16]	230.00	96.52	2	4.31	3.04	2.53	2.45	2.12	1.92
[16]	250.00	86.19	7	2.39	1.28	2.05	1.96	1.33	1.43
[16]	250.00	103.42	4	1.93	1.01	5.04	4.51	3.18	3.41
[30]	270.00	96.26	4	2.21	0.88	2.52	0.30	3.13	0.34
[30]	270.00	111.46	5	2.50	1.44	5.34	0.35	0.84	0.36
All data			45	2.73	1.48	2.02	1.22	1.12	0.90

[a] $\mathrm{AAD}P = \left[\frac{1}{N}\sum_{i=1}^{N}|P_i^{\exp} - P_i^{cal}|/P_i^{\exp}\right]\times 100$; [b] $\mathrm{AAD}y = \left[\frac{1}{N}\sum_{i=1}^{N}|y_i^{\exp} - y_i^{cal}|\right]\times 100$

First of all, a successful EOS should be available for modelling the liquid–vapour properties for non-critical conditions. One set of BIP must be fitted firstly for best agreement of the EOS with experimental data outside the critical and retrograde condensation region. Then, another set of BIP should be obtained for reproducing accurately the critical curves of binary subsystems.

If this work of fitting has been done with success, the experimental immiscibility curves must be compared with the immiscibility curves calculated by the EOS with non-critical BIP. Fig. 5 illustrates the possible problems that may arise for binary systems. Isothermal bubble and dew curves are plotted in pressure-composition diagrams. The dotted line represents the curves calculated by the EOS with non-critical BIP, whereas the solid line represents the experimental immiscibility curves. The three main types of vapour–liquid equilibria (VLE) calculations are considered here (bubble pressure, flash and dew pressure calculations). In Fig. 5(A), the temperature (T^*) and the mole fraction of the volatile component (x^*) are given for a bubble pressure calculation. A VLE solution, shown by an empty circle, does exist. However, this VLE point cannot be reached with our method. Indeed, the x^* composition is located outside the range of composition predicted by the EOS with non-critical BIP for the bubble curve. Thus, the ξ parameter cannot be estimated. In Fig. 5(B), the T^* temperature and the P^* pressure are fixed for a flash calculation. But, the P^* pressure exceeds the critical pressure calculated by the EOS with non-critical BIP. As a consequence, the solution cannot be found by a flash calculation. Fortunately, in this case, the solution can be approximated by performing several bubble pressure calculations. Another type of problem occurs when a bad ξ interpolation parameter has been obtained after a VLE calculation with non-critical BIP. This problems arises, for example, in Fig. 5(C), where the T^* temperature and the y^* composition of the vapour are fixed for a dew pressure calculation. The VLE solution lies in the retrograde condensation region, near the critical point. But, the VLE calculation with non-critical BIP leads to a point on the dew curve (filled circle) far outside the critical region. Thus, a value close to zero for the ξ interpolation parameter is found by using Eqs. (6) and (7a), whereas a value close to one would be expected. This problem can be bypassed too by doing bubble pressure or flash calculations instead of dew pressure calculations.

Such problems are expected to be rare. The liquid–vapour immiscibility region calculated by an EOS with non-critical BIP extends very often over the experimental immiscibility field. Thus, in most cases, there is no problem for estimating the ξ parameter from a VLE calculation with non-critical BIP. In the CO_2–CH_4–N_2 system, no serious problem was met. Only, dew pressure calculations could fail in the retrograde condensation region, as illustrated in Fig. 5(C). Indeed, the calculated critical points of the CO_2–CH_4 and CO_2–N_2 system are always shifted to CO_2-poorer concentrations with respect to experimental critical points. But, as explained above, VLE points in the retrograde condensation region can be calculated by a bubble pressure calculation.

In summary, our approach can be applied to any system that fulfills the following conditions: (1) an EOS can reproduce the experimental data points of VLE by using non-critical BIP; (2) the critical curve can be reproduced with a good accuracy with the same EOS, but with a different set of BIP; (3) the immiscibility region predicted with non-critical BIP includes the experimental immiscibility region. After these conditions have been checked for the system under investigation, it remains to define an interpolation function between non-critical and critical BIP. For the CO_2–CH_4–N_2 mixture, the ξ interpolation function, as defined by Eq. (7), has been used. The following values for s and A, 1.05 and 0.5, have been estimated for the CO_2–CH_4–N_2 system, and they are found to give satisfactory results. But another values could be required for modelling the VLE in the transition region between non-critical and critical conditions of other systems.

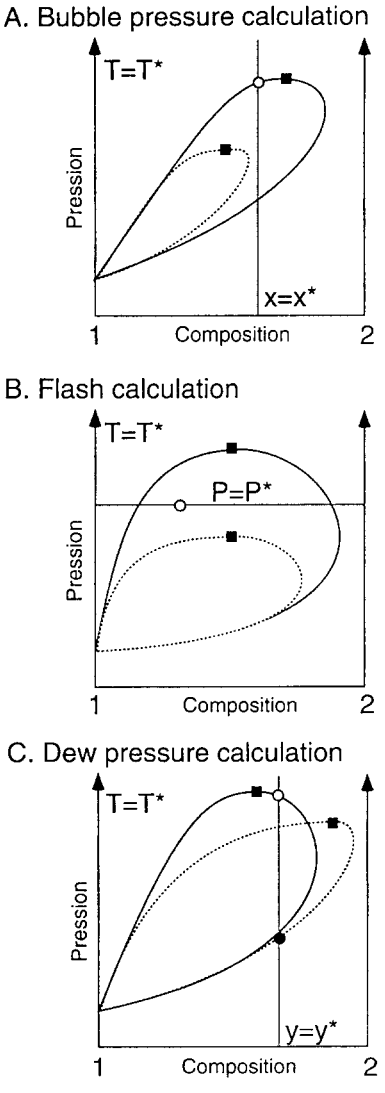

Fig. 5. Illustration of possible mismatches of our system. Fictive isothermal Px projections of the liquid-vapour immiscibility field are given here for a binary system (1–2). The solid line represents the experimental biphasic liquid-vapour region, that should be reproduced as closely as possible with our method. The dashed line delimits the immiscibility field calculated by an EOS with noncritical BIP. This dashed curve indicates the range of possible pressure-composition values that are obtained after a VLE calculation with noncritical BIP. Critical points on these immiscibility curves are indicated by full squares. The empty circle on the solid curve is an example of VLE point that cannot be calculated with our approach. A, A bubble pressure calculation cannot be done here with the given T^* temperature and x^* liquid composition. Indeed, the EOS with noncritical BIP fails to predict a VLE state, and thus no ξ distance can be determined. B, A flash calculation cannot be performed here with the given T^* temperature and P^* pressure. The P^* pressure is greater than the critical pressure (P_c) calculated by the EOS with noncritical BIP. Thus, no VLE state can be calculated with a flash calculation at the first step of our algorithm. C, A dew pressure calculation can be carried out with the given T^* temperature and y^* vapour composition, but leads to an uncorrect solution (represented by a filled circle), as it is characterized by a ξ value close to zero (noncritical conditions).

6. Conclusion

It is shown that cubic EOS provide a convenient framework for modelling liquid–vapour equilibria for non-critical and critical conditions. Two best-fitting sets of BIP have been determined from experimental data in and outside the critical region for the binary CO_2–N_2 and the CO_2–CH_4 system. One BIP on the a is sufficient for predicting liquid–vapour equilibria outside the critical region. On the contrary, two BIP on the a and b parameters are necessary for representing the critical curve of binary systems with sufficient accuracy. Effective BIP applied to the system are allowed to vary between both non-critical and critical sets of BIP. The continuity is ensured by an interpolation parameter, which is a function of the distance from the critical state. The interpolation parameter is obtained by an *a priori* liquid–vapour calculation, which provides an estimate of the ratio of the molar volumes of coexistent liquid and vapour. Our modified SRK EOS allows one to represent liquid–vapour equilibria with a good accuracy. Prediction of liquid–vapour equilibria are significantly improved in the ternary CO_2–CH_4–N_2 system, in particular for near-critical conditions. It is believed that this method could be applicable to other mixtures of nonpolar molecules.

7. List of symbols

P	pressure
T	temperature
a	attractive parameter of the SRK EOS
b	covolume of the SRK EOS
x_i	mole fraction of the i component
S	objective function used for fitting BIP
k_a^{nc}	BIP for the a parameter for non-critical conditions
k_a^{c}	BIP for the a parameter for critical conditions
k_b^{nc}	BIP for the b parameter for non-critical conditions
k_b^{c}	BIP for the b parameter for critical conditions
ξ	interpolation function
v_r	ratio of molar volumes of coexistent liquid and gas
v_L	molar volume of the liquid
v_G	molar volume of the gas
N	number of experimental data
A	parameter of the ξ function
s	parameter of the ξ function
P^*	a fixed pressure
T^*	a fixed temperature
x^*	a fixed liquid mole fraction
y^*	a fixed vapour mole fraction

Acknowledgements

This work has been funded by Elf Aquitaine and CNRS, and has been carried out through the HCM network (CEE-DG XII-G) "Hydrothermal-metamorphic water-rock interactions in crystalline

rocks: a multidisciplinary approach based on paleofluid analysis". The article has greatly benefitted from a careful review of earlier drafts with Dr A.M. van den Kerkhof. Professor H. Renon, Dr H. Zhou and two anonymous reviewers who are thanked for their comments and suggestions for improving the manuscript.

References

[1] Thiéry, R., Vidal, J. and Dubessy, J., 1994. Geochim Cosmochim. Acta, 58: 1073–1082.
[2] Thiéry, R., van den Kerkhof, A.M. and Dubessy, J., 1994. Eur. J. Mineral., 6: 753–771.
[3] Heyen, G., 2nd World Congr. of Chemical Engineering, In: S.A. Newmann (Editor), Montreal, Que., 1981, p 175.
[4] Feroiu, V. and Geana, D., 1990. Fluid Phase Equilibria, 55: 263–270.
[5] Kreglewski, A. and Hall, K.R., 1983. Fluid Phase Equilibria, 15: 11–32.
[6] Huron, M.J., Dufour, G.N. and Vidal, J., 1977. Fluid Phase Equilibria, 1: 247–265.
[7] Peng, D.Y. and Robinson, D.B., 1977. AIChE J., 23: 137–144.
[8] Thiéry, R. and Dubessy, J., Proc. 4th Int. Symp. on Hydrothermal Reactions, Nancy, France, August 31–September 3, 1993, Institut Lorrain des Geosciences, Nancy, p. 259.
[9] Thiéry, R. and Dubessy, J., 13th IUPAC Conf. on Chemical Thermodynamics, Clermont-Ferrand, July 17–22, 1994, p 296.
[10] Firozabadi, A., 1994. Can. J. Chem. Eng., 72: 134–141.
[11] Soave, G., 1972. Chem. Eng. Sci., 27: 1197–1203.
[12] Vidal, J., 1978. Chem. Eng. Sci., 33: 787–791.
[13] Asselineau, L., Bogdanic, G. and Vidal, J., 1979. Fluid Phase Equilibria, 3: 273–290.
[14] Thiéry, R., Computers & Geosciences, 1996, in press.
[15] Al-Sahhaf, T.A., Kidnay, A.J. and Sloan, E.D., 1983. Ind. Eng. Chem. Fundam., 22: 372–380.
[16] Al-Sahhaf, T.A., 1990. Fluid Phase Equilibria, 55: 159–172.
[17] Al-Wakeel, 1976. Diss. TU Berlin.
[18] Arai, Y., Kaminishi, G. and Saito, S., 1971. J. Chem. Eng. Jap., 4: 113–122.
[19] Chang, S.D. and Lu, B.C.Y., 1967. Chem. Eng. Prog. Symp. Ser., 63: 18–27.
[20] Cines, M.R., Roach, J.T., Hogan, R.J. and Roland, C.H., 1953. Chem. Eng. Prog. Symp. Ser., 49: 1–100.
[21] Davalos, J., Anderson, W.R., Phelps, R.E. and Kidnay, A.J., 1976. J. Chem. Eng. Data, 21: 81–84.
[22] Donnelly, H.G. and Katz, D.L., 1954. Ind. Eng. Chem., 46: 511–517.
[23] Hwang, S.C., Lin, H.M., Chappelear, P.S. and Kobayashi, R., 1976. J. Chem. Eng. Data, 21: 493–497.
[24] Kaminishi, G.I., Arai, Y., Saito, S. and Maeda, S., 1968. J. Chem. Eng. Jap., 1: 109–116.
[25] Kidnay, A.J., Miller, R.C., Sloan, E.D. and Hiza, M.J., 1985. J. Phys. Chem. Ref. Data, 14: 681–694.
[26] Mraw, S.C., Hwang, S.C. and Kobayashi, R., 1978. J. Chem. Eng. Data, 23: 135–139.
[27] Muirbrook, N.K. and Prausnitz, J.M., 1965. AIChE J., 11: 1092–1097.
[28] Neumann, P.N.A. and Walch, W., 1968. Chem. Eng. Tech., 40: 241–244.
[29] Parrish, W.R. and Hiza, M.J., 1974. Adv. Cryog. Eng., 19: 300–308.
[30] Somait, F.A. and Kidnay, A.J., 1978. J. Chem. Eng. Data, 23: 301–305.
[31] Stryjek, R., Chapelear, P.S. and Kobayashi, R., 1974. J. Chem. Eng. Data, 19: 334–339.
[32] Yorizane, M., Yoshimura, S., Masuoka, H., Myano, Y. and Kakimoto, Y., 1971. J. Chem. Eng. Jap., 30: 174–176.
[33] Zenner, G.H. and Dana, L.I., 1963. Chem. Eng. Prog. Symp. Ser., 59: 36–41.
[34] Xu, N., 1992. Fluid Phase Equilibria, 81: 175–180.
[35] Bian, B., Wang, Y., Shi, J., Zhao, E. and Lu, B.C.Y., 1993. Fluid Phase Equilibria, 90: 177–185.
[36] Wei, M.S.W., Brown, T.S., Kidnay, A.J. and Sloan, E.D., 1996. J. Chem. Eng. Data, 40: 726–740.
[37] van den Kerkhof, A.M., 1990. Geochim. Cosmochim. Acta, 54: 621–629.